



# Neutron scattering and hydrogenous materials

Advances in neutron scattering instrumentation along with new sources are providing exciting new opportunities to study increasingly complex issues in materials research. Here we provide a basic introduction into the properties of the neutron that make it a nearly ideal probe of materials. We then describe recent examples that demonstrate how these properties have been exploited to study the dynamics of hydrogen and water in a variety of materials.

Dan A. Neumann

*NIST Center for Neutron Research, National Institute of Standards and Technology, Gaithersburg, MD 20899-8562, USA*

*E-mail: [dan@nist.gov](mailto:dan@nist.gov)*

The unique properties of the neutron, which is a charge neutral subatomic particle, make it a nearly ideal particle for scattering investigations of materials. The enormous utility of the neutron in studies of dynamical phenomena stems from the ability to measure the momentum and energy transferred during the neutron scattering event simultaneously, thereby providing the experimentalist with information in both the spatial and time domains, respectively. Thus not only are neutron inelastic scattering techniques sensitive to the frequencies associated with a fluctuating object, they are also sensitive to the structure or geometry of the excitation.

Neutrons interact directly with the atomic nucleus. Therefore the strength of the scattering depends not only on the element, but also on the specific isotope. Moreover, the details of the nuclear and nuclear spin interactions responsible for neutron scattering lead to scattering cross sections that vary in a seemingly random manner from isotope to isotope. These cross sections depend only weakly on the atomic number (Fig. 1). Thus neutron scattering is far more sensitive to light elements located near heavy ones than are methods, such as X-ray scattering, that depend largely on electronic interactions. More importantly, one

can often adjust the scattering from a particular system through isotopic substitution. This is particularly effective for hydrogen since a proton scatters neutrons very strongly, and for many systems the scattering from hydrogen dominates the spectrum. Deuterium, on the other hand, scatters relatively weakly. Thus one is often able to determine the dynamics of selected constituents of hydrogenous materials via isotopic labeling.

Equally important, though beyond the scope of this article, is the magnetic scattering of neutrons, which allows the determination of magnetic structures and spin dynamics with a sensitivity surpassing any other technique. These capabilities are often crucial for obtaining a detailed picture of atomic and nanoscale dynamics in materials, and elevate neutrons to a unique status compared with other spectroscopic tools available to materials researchers.

The theory of inelastic neutron scattering is well developed and chronicled in a number of excellent books<sup>1-5</sup> and it will not be repeated here. It should be emphasized that the interaction of neutrons with materials is relatively simple; this allows the expected scattering spectra to be calculated easily from theories and models. This fact has recently been exploited to compare neutron data directly to a variety of first-

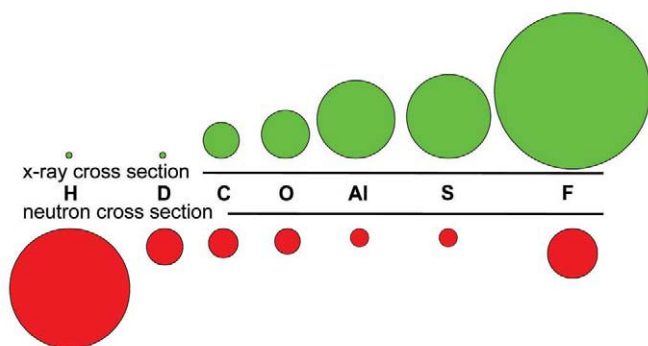


Fig. 1 Schematic of the relative total scattering cross sections for neutrons and X-rays for several elements and isotopes. Note the large scattering power of neutrons. (Courtesy of Muhammad Arif, NIST.)

principles calculations and molecular-dynamics simulations. In fact, the time and length scales accessible to molecular-dynamics simulations correspond almost exactly with those probed by neutron spectroscopy. Thus neutron scattering provides a powerful test of these methods<sup>6-7</sup>.

Atomic and molecular motions in materials occur over a wide range of time and length scales. Over the last three decades, neutron instrumentation has been developed and improved to the point where inelastic scattering methods now cover many orders of magnitude in time, spanning subpicosecond to beyond 100 ns time scales. These advances allow researchers to examine a rich variety of phenomena ranging from vibrational spectroscopy through diffusion to relaxations. Instrumentation for neutron inelastic scattering is tailored to a particular energy and momentum (wavevector  $Q$ ) transfer region. Fig. 2 shows the phase space that is accessible by a variety of spectrometers at the NIST Center for Neutron Research. The instrumentation covers seven orders of magnitude in energy and more than three in length scale. Note that as one goes to slower motions the length scale probed by the instrumentation increases. This is intentional since longer length-scale motions tend to be slower.

Together, these fundamental properties of the neutron make it unmatched as a tool to elucidate the dynamics of materials. To date, neutrons have made numerous and invaluable contributions to understanding the key interactions in a wide variety of systems. In this article, we will describe several recent examples of research that highlight the usefulness of neutrons to study the dynamics of hydrogen and water in a broad class of materials.

## Hydrogen storage materials

Developing safe, cost-effective, and practical means of storing hydrogen is crucial for the advancement of hydrogen and fuel cell technologies. The discovery by Bogdanovic and Schwickardi<sup>8</sup> that Ti enhances reversible hydrogen sorption in Na alanates opened up a new prospect for lightweight hydrogen storage. Neutron vibrational spectroscopy<sup>9,10</sup>, the neutron analog of Raman spectroscopy, is the ideal probe of the interactions of hydrogen with the material matrix in

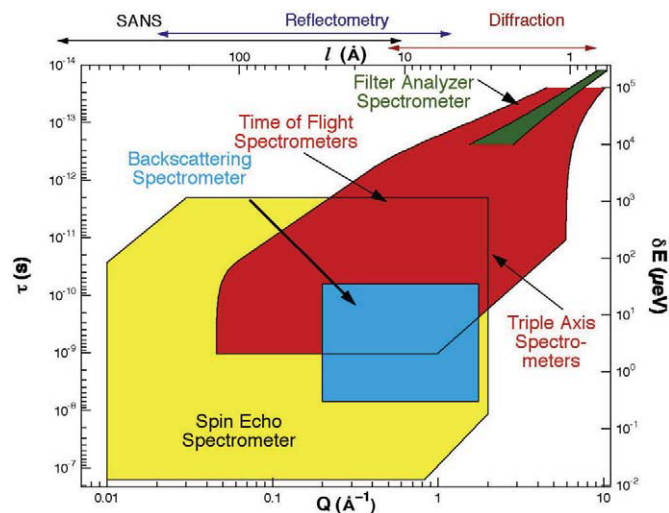


Fig. 2 Phase space regions covered by neutron inelastic scattering instruments at the NIST Center for Neutron Research. The time scale of a particular motion is related to the energy transferred in the scattering process through a Fourier transform. Similarly the momentum transferred  $Q$  is related to the length scale probed. Major neutron centers worldwide have developed instrumentation that covers similar regions of phase space. (Courtesy of Ron Cappelletti, NIST.)

any hydrogen storage material. First-principles calculations provide an ideal complement to neutron scattering because the intensities of the features in a neutron vibrational spectrum depend only on the amplitudes of the vibrations of the various atoms for that vibrational mode weighted by the cross section for that particular atom. This means that the entire neutron spectrum can be directly calculated from the dynamical matrix since the eigenvalues give the frequencies and the eigenvectors give the amplitudes of vibration. The dynamical matrix, which is comprised of force constants for small displacements of the individual atoms from their equilibrium positions, can be directly obtained from first-principles calculations by slightly displacing each atom in turn.

Fig. 3 shows the measured vibrational spectrum of sodium alanate,  $\text{NaAlH}_4$ , which exhibits several sharp phonon bands up to 250 meV<sup>11,12</sup>. It also shows the one-phonon spectrum, calculated with the plane-wave implementation of the generalized gradient approximation<sup>14</sup> to density functional theory (DFT) using the ABINIT package<sup>15,16</sup>. This calculated spectrum fails to explain several features in the data. However, the inclusion of two-phonon scattering yields a spectrum that is in very good agreement with the experimental one. Without the results from DFT, these multiphonon contributions could have easily been mistaken for scattering from single phonons. The calculations also provide the assignments of the phonon bands seen in Fig. 3. The low energy modes are whole-body translations of the  $\text{AlH}_4$  tetrahedra. The strong features around 50 meV are a result of the torsional modes of the tetrahedra. Because of the large scattering cross section for H and the large H displacements of these modes, they would be expected to lead to some

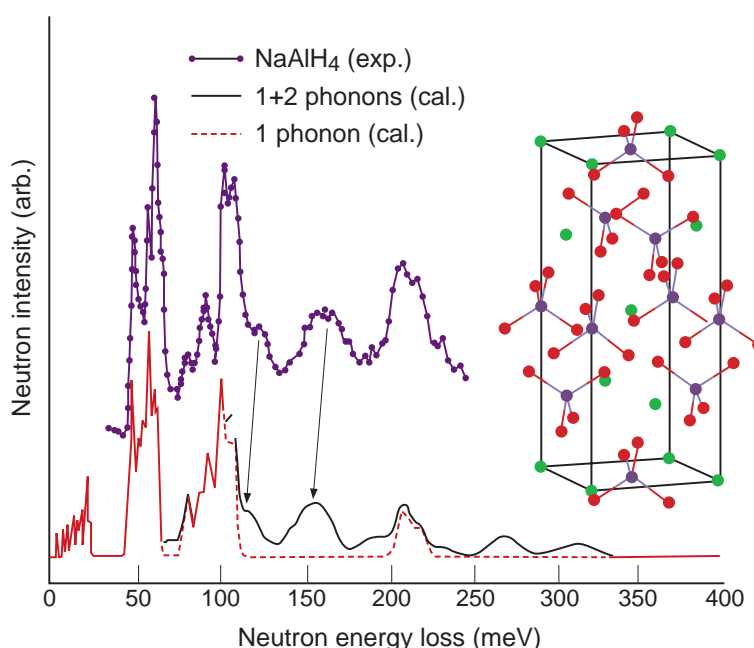


Fig. 3 Measured (top) and calculated (bottom) neutron vibrational spectra of  $\text{NaAlH}_4$ . The calculated 1 and 1+2 phonon contributions are shown as the red dashed and black solid line, respectively. The structure of  $\text{NaAlH}_4$  determined from neutron diffraction data<sup>12,13</sup> is shown in the inset. The blue atoms (Al) and the red atoms (H) form  $\text{AlH}_4$  tetrahedra. The Na atoms are shown in green. ( $1 \text{ meV} \sim 8 \text{ cm}^{-1}$ )

of the most intense peaks in the spectra. The peaks above 200 meV arise from various Al-H stretching modes. The features between 75 meV and 125 meV arise primarily from H-Al-H bending modes with some hybridization to stretches and rotations of the tetrahedra.

While no clear spectral differences were noted when the Na alanate was doped with Ti, the agreement between the calculations and the experiment give confidence in the total energies that are obtained from the DFT calculations. These calculations indicate that Ti doping in  $\text{NaAlH}_4$  is energetically favorable and that Ti prefers to substitute for Na. The Ti-H interactions not only weaken the Al-H bonds, but result in the incorporation of additional hydrogen in the vicinity of the Ti dopant. Additional calculations for thick slabs of Ti-doped  $\text{NaAlH}_4$  predict that it is even more energetically favorable for Ti to remain on the surface, substitute for Na, and attract H atoms to its vicinity<sup>17</sup>. Thus the neutron vibrational spectroscopy lends considerable credibility to density functional calculations that explain the catalytic effect of Ti on H incorporation and release in these materials.

Hydrogen can also be safely stored by physisorption of molecular hydrogen rather than by the sorption of atomic hydrogen into a metallic host. While it is well known that neutron diffraction can be used to locate the hydrogen in crystalline materials, inelastic neutron scattering is also important for understanding the physisorption of hydrogen molecules. This is because neutron spectroscopy can be used to observe the quantized rotational levels, i.e. transitions between the  $j = 0$  and  $j = 1$  rotational levels or alternatively conversions between *ortho* and *para* hydrogen. Observation of a rotational transition not only demonstrates that hydrogen is present as  $\text{H}_2$ , but any shift in energy

from 14.7 meV, the value for free rotations, yields information on the strength and symmetry of the rotational potential<sup>18</sup> and, therefore, can yield the number of different adsorption sites. This information on the characteristics of the binding sites can be invaluable for optimizing the characteristics of  $\text{H}_2$  physisorption for potential hydrogen storage applications. Thus neutron scattering has been used extensively to study the rotational dynamics of  $\text{H}_2$  in a variety of materials including carbon nanotubes<sup>19-22</sup>,  $\text{C}_{60}$ <sup>23</sup>, nanoporous Ni phosphates<sup>24</sup>, and zeolites<sup>25,26</sup>.

Metal-organic framework (MOF) materials are comprised of metal-oxide clusters connected by organic linkers. Because of their tunable pore size and functionality, these new nanoporous systems show promise for hydrogen storage applications<sup>27-33</sup>. Thus it is not surprising that inelastic neutron scattering has been used to study the rotational levels of  $\text{H}_2$  adsorbed in several different MOFs including MOF-5. This particular material has clusters of four corner-joined  $\text{ZnO}_4$  tetrahedra linked by organic 1,4-benzenedicarboxylate linkers. At relatively low hydrogen loadings (four and eight  $\text{H}_2$  per four Zn), Yaghi, Eckert, and coworkers<sup>34,35</sup> observed peaks at 10.3 meV and 12.1 meV, which are assigned to transitions from the  $j = 0$  to  $j = 1$  rotational levels for hydrogen in sites near the Zn atoms and the linker, respectively. The shift from 14.7 meV implies rotational barriers of 1.6 kJ/mol and 1.0 kJ/mol for the two sites. As the loading is increased, the intensity of the second peak grows and eventually splits into four different peaks, which indicates that there are a variety of nearly isoenergetic adsorption sites. At the same time, other peaks appear that can be assigned to various transitions in the manifolds containing the first two transitions. Finally, a peak indicative of free  $\text{H}_2$  rotations appears.

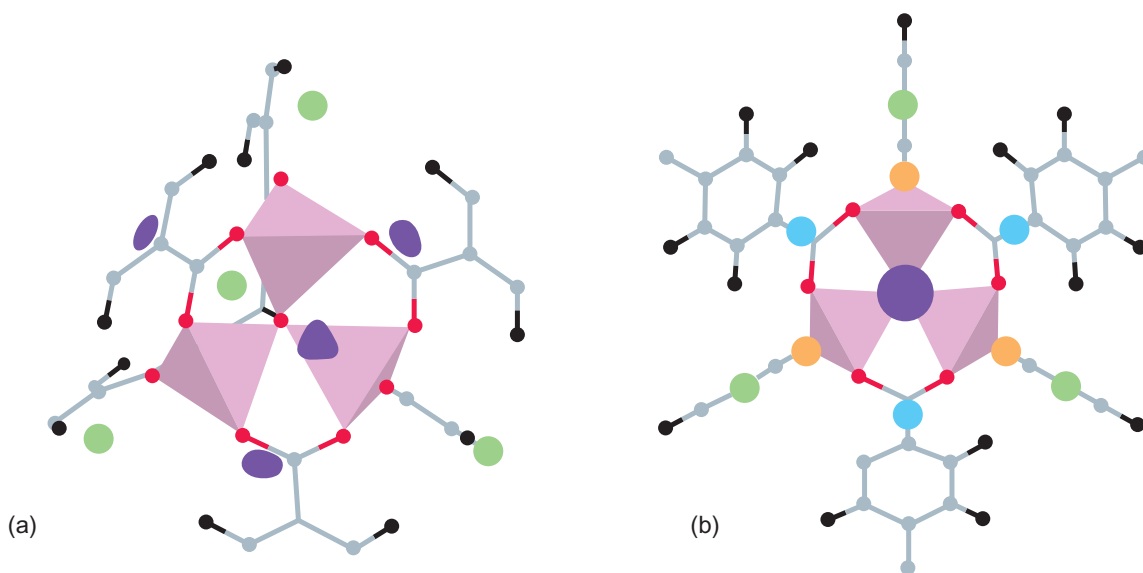


Fig. 4 The hydrogen adsorption sites for  $H_2$  in MOF-5. The  $ZnO_4$  tetrahedra are shown in pink and the organic linkers in gray and black: (a) the first (blue) and second (green) absorption sites, respectively; (b) a view along the three-fold axis, showing the first four adsorption sites. The  $ZnO_2$  sites are shown in brown and the sites above the benzene rings in light blue.

Recent neutron powder diffraction measurements at low temperature along with Fourier difference methods (Fig. 4) add detail to these assignments<sup>36</sup>. These results demonstrate that the  $ZnO_4$  cluster is responsible for most of the hydrogen adsorption, while the organic linker plays a secondary role. The first site filled, shown in blue in Fig. 4, is termed the 'cup site' and is located in the cup formed by the  $ZnO_4$  tetrahedra. The second site, shown in green, is directly above the triangles of oxygen atoms, which are directly opposite the oxygen shared by the four tetrahedra. These sites give rise to the first two peaks observed in inelastic scattering experiments. The next molecules, shown in brown, reside above the line defined by adjacent oxygen atoms, and in the sites above the benzene ring, shown in light blue. These hydrogen molecules must have a very small barrier to rotation and thus probably contribute to the splitting of the peak in the inelastic scattering at 12.1 meV. At very high loadings, the hydrogen molecules rearrange themselves in order to more completely fill the pore space. These networks of  $H_2$  molecules display intermolecular distances of 3.0 Å, which is significantly shorter than the intermolecular distances of 3.6 Å in pure solid hydrogen.

## Dynamics of nanoconfined water

Water is a fascinating substance<sup>37,38</sup>. Its remarkable properties are primarily due to the strong hydrogen bonding between water molecules, which leads to very different thermal properties than one would have in a simple liquid. Thus the dynamics of water, which reflect the intermolecular interactions, are of particular interest. Quasielastic neutron scattering has been applied to study the dynamics of not only bulk water<sup>39-40</sup>, but to water confined in a variety of nanostructured materials<sup>41-52</sup>. Recently, Chen and coworkers<sup>53-57</sup> have

performed an elegant series of quasielastic neutron scattering experiments that probe the dynamics of water in mesoporous silica.

Angell<sup>58</sup> has proposed that liquids can be classified according to the temperature dependence of their viscosity as they approach a glass transition. For 'fragile' liquids such as supercooled water, the temperature dependence of the structural relaxation time  $\tau$  follows a Vogel-Fulcher-Tammann (VFT) law:  $\tau = \tau_0 \exp[DT_0/(T - T_0)]$ , where  $T_0$  is the temperature of the apparent divergence of the relaxation time and  $D$  is a constant that provides a measure of fragility. On the other hand, in strong liquids the temperature dependence of  $\tau$  obeys the standard Arrhenius law:  $\tau = \tau_0 \exp(E_A/RT)$ , where  $E_A$  is the activation energy for the relaxation process and  $R$  is the gas constant. Based on thermodynamic arguments, it has been proposed that supercooled water would undergo a fragile-to-strong transition between two liquid phases at around 228 K<sup>59-62</sup>. However, supercooled bulk water reaches its homogeneous nucleation point and crystallizes into ice at 235 K, thereby preventing the observation of the proposed liquid-to-liquid transition<sup>63</sup>.

It is well known that confinement of liquids in small pores suppresses freezing. Chen and coworkers have exploited this by using micelle-templated mesoporous silica matrices to suppress freezing and supercool water to 200 K. These materials, referred to as MCM-41-S, have well-ordered, cylindrical pores arranged in two-dimensional hexagonal arrays. The pores have a uniform diameter of ~1.4 nm. The quasielastic spectra of water confined in pores is well-described using a 'relaxing cage model'<sup>64,65</sup>. In this model, the water is trapped in a cage of other water molecules that gradually relax, forming new cages. The heterogeneity of the dynamics leads to a stretched exponential relaxation of the location of each water molecule. This model allows



one to extract a variety of parameters including, most importantly, the average translational relaxation time  $\langle\tau_T\rangle$ , which is the time that it takes for a hydrogen-bonded cage surrounding a water molecule to relax. Measurements were required over nearly four orders of magnitude in time, which required the use of two different neutron spectrometers. Fig. 5a, which is an Arrhenius-type plot of  $\log\langle\tau_T\rangle$  versus  $T_0/T$ , clearly shows a transition from fragile-to-strong behavior at  $T_L = 224$  K and ambient pressure<sup>56-57</sup>. This is the most direct observation of a liquid-to-liquid transition in confined water reported to date.

The anomalies in the thermodynamic quantities also indicate the possible existence of a low-temperature critical point near this transition temperature, but at somewhat elevated pressure. Figs. 5a and 5b show a cusp-like fragile-to-strong transition around 220 K for pressures up to 0.8 kbar. However, at higher pressures (Fig. 5c), this transition becomes rounded and it is not possible to define a transition temperature. Fig. 6 displays the phase diagram in the pressure-temperature plane. The fragile-to-strong transition temperature is denoted as  $T_L$  and the homogeneous nucleation temperature as  $T_H$ . The  $T_L$  line approximately tracks the  $T_H$  line, and appears to terminate when it intersects the  $T_H$  line at about 1.6 kbar and 200 K. Above this pressure, it is no longer possible to identify the fragile-to-strong transition. Chen and coworkers<sup>57</sup> argue that the fragile-to-strong dynamic transition, denoted by  $T_L$ , is a liquid-liquid transition, and that the high-temperature phase is a high-density liquid where the local hydrogen bond network is not fully developed, while the low-temperature, low-density liquid has a more locally ice-like hydrogen bond network. Whether or not this is truly a liquid-to-liquid transition, it is clear that the state of water continues to be a very interesting subject and that neutron scattering will continue to play an important role in elucidating its structure and dynamics.

## The hydration of cement

More than 800 million metric tons of Portland cement are produced each year, making concrete the most widely used material on Earth. Despite this and even though its social and economic importance is greater than that of Si, the fundamental structure of hydrated Portland cement is still poorly understood. Making the challenge even greater, the structure, molecular composition, and physical properties of cement vary considerably during hydration<sup>66</sup>. The goal of understanding the key structural features and their temporal evolution during the hydration reaction has been frustrated by the lack of suitable experimental methods for exploring the key nanocrystalline and amorphous calcium silicate hydrate (CSH) phases that give concrete its useful properties. Because quasielastic neutron scattering is particularly sensitive to hydrogen, it is possible to use neutron methods to quantitatively and nondestructively follow the state of the water as the hydration reaction proceeds<sup>67-76</sup>.

Portland cement consists of many components. It is crucial to understand how these components interact during the reaction and

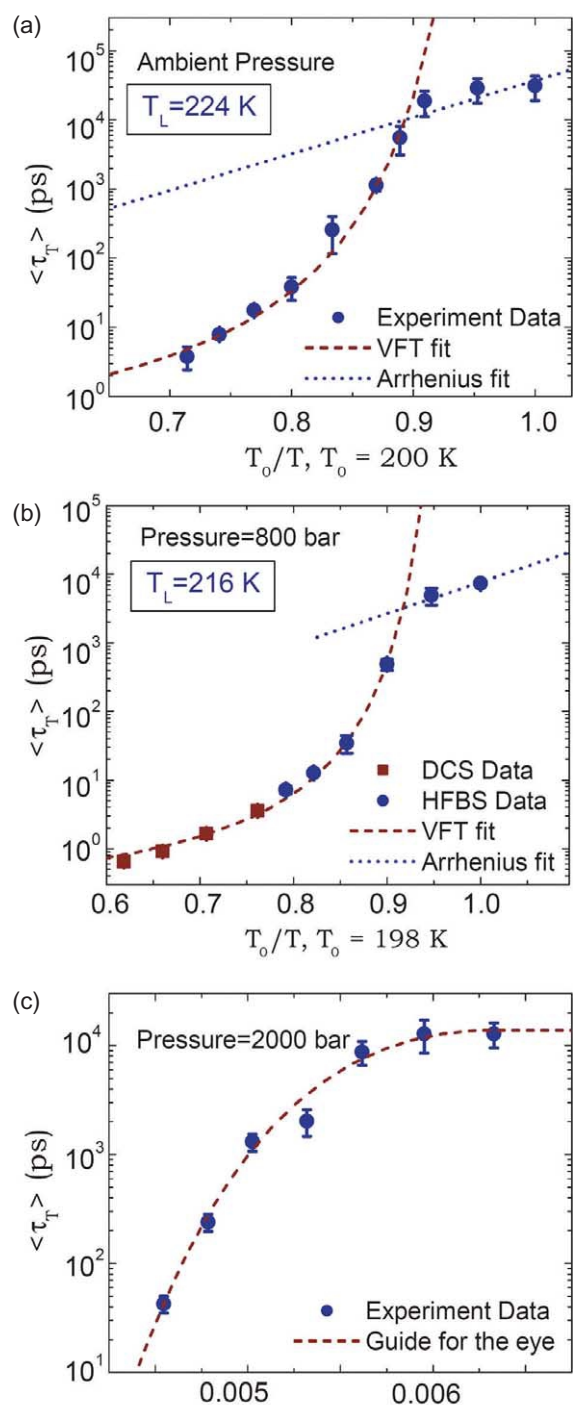


Fig. 5 Temperature dependence of  $\log\langle\tau_T\rangle$  as a function of  $T_0/T$ , where  $T_0$  is the glass transition temperature in the VFT law. Data at ambient pressure (1 bar), 0.8 kbar, and 2.0 kbar are shown in panels (a), (b), and (c), respectively. There is a clear transition from VFT to Arrhenius behavior in (a) and (b) with the transition temperature  $T_L$  indicated. There is no clearly identifiable transition in panel (c).

contribute to the final CSH. Recently Peterson and coworkers<sup>75</sup> have undertaken a series neutron scattering studies on mixtures of tricalcium silicate ( $\text{Ca}_3\text{SiO}_5$ , abbreviated as C3S), the most important and

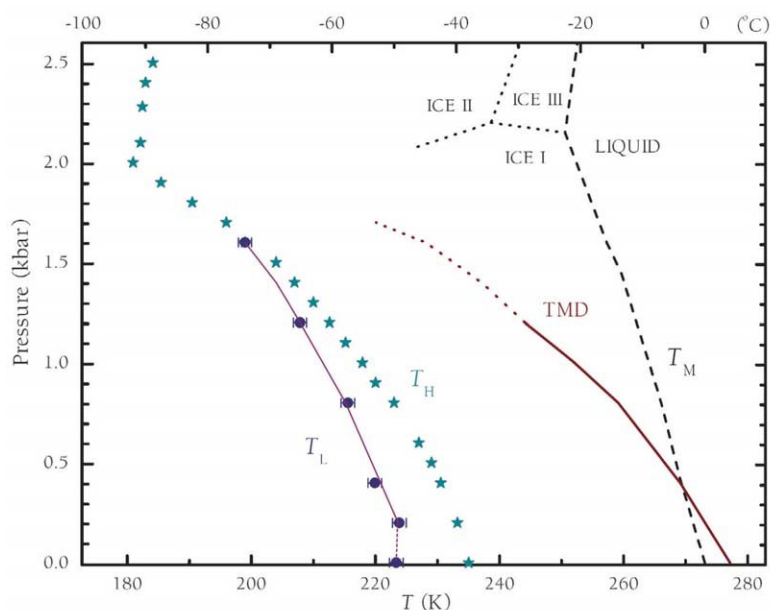


Fig. 6 Phase diagram in the pressure-temperature plane:  $T_L$  (solid circles) is the fragile-to-strong transition temperature that terminates in a critical point at about 1.6 kbar and 200 K where it intersects the homogeneous nucleation temperature line, denoted as  $T_H$ . The temperature of maximum density line, denoted as TMD, is also shown. The  $T_L$  line is roughly parallel to the TMD line, suggesting that the low temperature phase has a lower density.

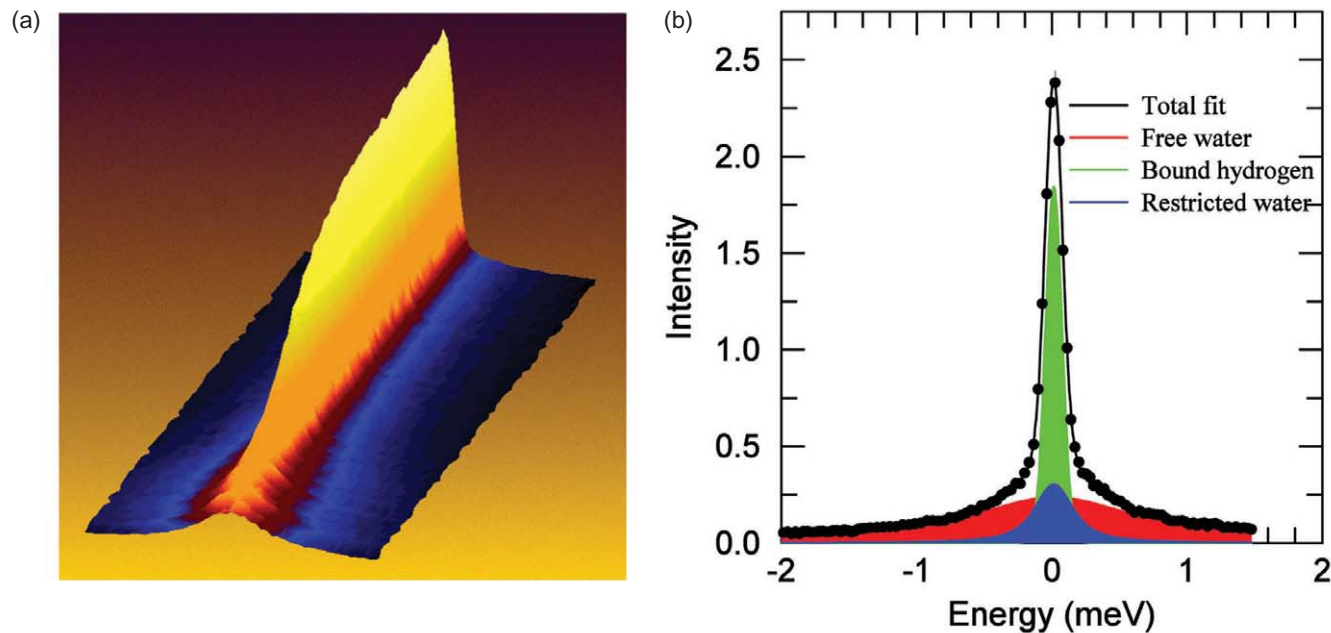


Fig. 7 (a) A series of quasielastic neutron scattering spectra for a period of 30 hours. Three distinct periods are visible. First there is a dormant period during which the scattering is broad and consistent with that of bulk water. Next there is a period during which the reaction occurs quickly, referred to as the nucleation and growth regime. The reaction then slows and is governed by the rate at which water can diffuse through the hydration products to reach unreacted C3S and C2S. The integrated intensity is independent of time indicating that no hydrogen is lost during the reaction. (b) A typical fit to a quasielastic spectrum at a particular time. The red component is that of bulk water. The blue component is due to water in small pores and on internal surfaces. The green component is hydrogen that is immobile on the scale of the instrumental resolution. The BWI is defined as the sum of the green and blue components over the total.

abundant component of Portland cement, and dicalcium silicate ( $\text{Ca}_2\text{SiO}_4$ , abbreviated as C2S), which is the second most abundant component. Together, these two components typically account for

approximately 80 wt.% of Portland cement. C3S reacts with water on a time scale that is familiar for the setting of concrete. C2S is much less reactive.

A typical series of quasielastic scattering curves representative of the first 30 hours of the hydration reaction is shown in Fig. 7a. After an initial dormant period, two hydration mechanisms can be identified: (a) nucleation and growth of products, when the cement starts to set, and (b) diffusion-limited hydration, occurring when the permeability of the reaction products limits the ability of water to reach the hydrating particles. A quasielastic spectrum for a particular time is shown in Fig. 7b. The kinetics of the hydration reaction are characterized using the 'bound water index' (BWI), which is determined from the ratio of the amount of less mobile hydrogen (the sum of the blue and green components) relative to the total hydrogen in the system. As hydrogen is initially only present in water and is transferred to the reaction products during the hydration of C3S and C2S, the BWI is essentially a measure of the amount of product. Thus a plot of BWI versus time describes the kinetics of the hydration reaction. The BWI curves for C3S and C2S mixtures indicate that, for intermediate compositions, the reaction cannot be described as a linear combination of the end points. The kinetics can be parameterized by fitting the BWI to a kinetic model, allowing the hydration kinetics to be quantified<sup>73-76</sup>. For example, the amount of product formed during the nucleation and growth phase *A* can be determined. *A* is useful for predicting early strength development, as the amount of product (as well as type) correlates with cement strength. Another important parameter is the effective diffusion constant  $D_i$ , which limits the reaction rate in the diffusion-limited regime.  $D_i$  correlates with the permeability of the CSH<sup>72</sup>.

Fig. 8 shows that both *A* and  $D_i$  exhibit a maximum for a mass fraction of C3S between 80% and 95%. Thus the hydration reaction

actually progresses faster when one adds a small amount of relatively unreactive C2S. This can be attributed to the presence of additional nucleation sites provided by the less reactive C2S, thereby allowing some nucleation of CSH to occur at sites remote from the C3S. The similar atomic composition and hydration products for C2S and C3S combine to make the C2S surface suitable for the nucleation and growth of products from the hydrating C3S. Providing these nucleation sites using C2S rather than inert particles such as silica is advantageous because C2S not only provides a favorable template, but reacts itself, albeit slowly. Therefore C2S enhances the later strength of the paste<sup>75,76</sup>. Neutron scattering has identified the reason that commercial Portland cement has been developed through more than 100 years of trial and error to have approximately the C3S to C2S ratio that optimizes the hydration reaction and the strength of concrete.

## Concluding remarks

Neutron scattering continues to play an ever-expanding role in elucidating the key dynamics of materials. Here we have discussed only a small segment of the myriad types of materials that have been studied using inelastic neutron scattering and the impact that scattering studies have had on our understanding of materials. In fact, we have only considered a single atom, namely hydrogen. The field is obviously much broader than space permits us to cover here.

The importance of neutron scattering will only continue to grow. Countries around the world recognize this and new neutron scattering facilities continue to be developed. Currently Australia<sup>77</sup>, China<sup>78,79</sup>, Germany<sup>80</sup>, Japan<sup>81</sup>, the UK<sup>82</sup>, and the USA<sup>83</sup> are all developing new

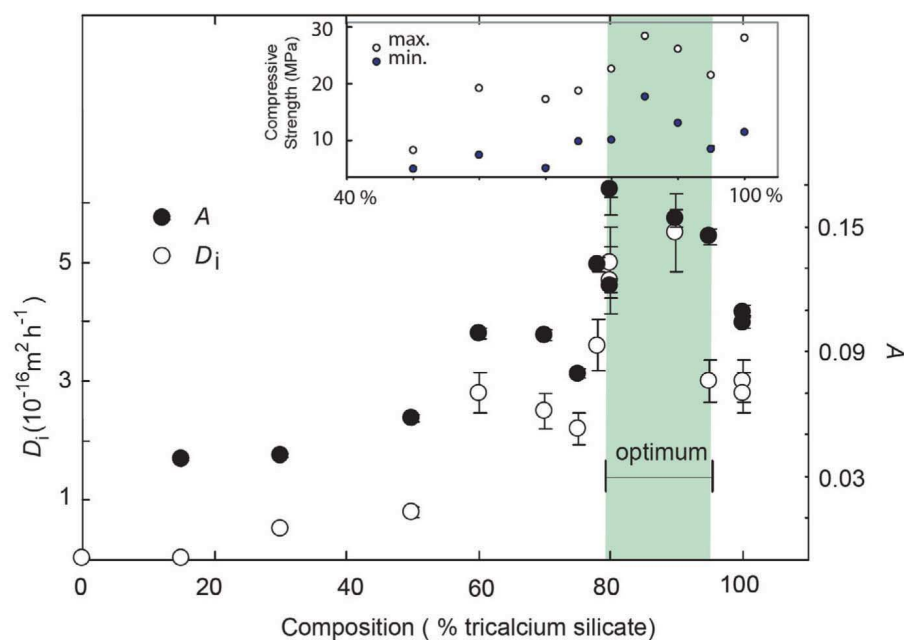



Fig. 8 Variation of the amount of product that would have been formed by nucleation and growth had it continued until the reaction was complete (*A*) and the diffusion coefficient ( $D_i$ ) with the weight per cent of C3S.

neutron sources or major new experimental facilities. The developments above, together with those at existing neutron centers, will increase the types of measurements that are feasible and allow scientists to bring the unique power of neutron scattering to bear on scientific questions that are beyond current capabilities. It is therefore an exciting time to be involved in neutron scattering research. 

## Acknowledgments

*I have greatly benefited from collaborations and other interaction with many colleagues over the years. I am also indebted to Jack Rush and Peter Gehring for critically reading this manuscript and to Ron Cappelletti for assistance with the figures. Some of the facilities used for the research described in this article are part of the Center for High Resolution Neutron Scattering, which is a partnership between the NIST Center for Neutron Research and the National Science Foundation under agreement DMR-0454672.*

## REFERENCES

1. Lovesey, S. W., *Theory of Thermal Neutron Scattering from Condensed Matter*, Clarendon Press, Oxford, UK, (1987)
2. Bacon, G. E., *Neutron Diffraction*, Clarendon Press, Oxford, UK, (1975)
3. Squires, G. L., *Introduction to the Theory of Thermal Neutron Scattering*, Cambridge University Press, (1978); republished by Dover Publications, Mineola, NY, USA, (1996)
4. Bee, M., *Quasielastic Neutron Scattering*, Adam Hilger, Bristol, UK, (1988)
5. Hempelmann, R., *Quasielastic Neutron Scattering and Solid State Diffusion*, Oxford University Press, Oxford, UK, (2000)
6. See the special issue on Neutron Scattering and Numerical Methods, *Chem. Phys.* (2000) **261** (1-2)
7. Tarek, M., et al., *Chem. Phys.* (2003) **292**, 435
8. Bogdanovic, B., and Schwickardi, M., *J. Alloys Compd.* (1997) **253**, 1
9. Copley, J. R. D., et al., *Can. J. Phys.* (1995) **73**, 763
10. Udovic, T. J., et al., *Nucl. Instrum. Methods A* (2004) **517**, 189
11. Íñiguez, J., et al., *Phys. Rev. B* (2004) **70**, 060101
12. Hauback, B. C., et al., *J. Alloys Compd.* (2003) **358**, 142
13. Ozolins, V., et al., *J. Alloys Compd.* (2004) **375**, 1
14. Perdew, J. P., et al., *Phys. Rev. Lett.* (1996) **77**, 3865
15. Gonze, X., et al., *Comput. Mater. Sci.* (2002) **25**, 478
16. <http://www.abinit.org>
17. Íñiguez, J., and Yildirim, T., *Appl. Phys. Lett.* (2005) **86**, 103109
18. Pauling, L., *Phys. Rev.* (1930) **36**, 430
19. Brown, C. M., et al., *Chem. Phys. Lett.* (2000) **329**, 311
20. Ren, Y., and Price, D. L., *Appl. Phys. Lett.* (2001) **79**, 3684
21. Narehood, D. G., et al., *Phys. Rev. B* (2002) **65**, 233401
22. Georgiev, P. A., et al., *J. Phys.: Condens. Matter* (2004) **16**, L73
23. FitzGerald, S. A., et al., *Phys. Rev. B* (1999) **60**, 6439
24. Forster, P. M., et al., *J. Am. Chem. Soc.* (2003) **125**, 1309
25. Nicol, J. M., et al., *J. Phys. Chem.* (1988) **92**, 7117
26. Eckert, J., et al., *J. Phys. Chem.* (1996) **100**, 10646
27. Li, H., et al., *Nature* (1999) **402**, 276
28. Eddaoud, M., et al., *Science* (2002) **295**, 469
29. Yaghi, O. M., et al., *Nature* (2003) **423**, 705
30. Ockwing, N. W., et al., *Acc. Chem. Res.* (2005) **38**, 176
31. Rowsell, J. L. C., et al., *J. Am. Chem. Soc.* (2004) **126**, 5666
32. Zhao, X., et al., *Science* (2004) **306**, 1012
33. Yang, Q., and Zhong, C., *J. Phys. Chem. B* (2005) **109**, 11862
34. Rosi, N. L., et al., *Science* (2003) **300**, 1127
35. Rowsell, J. L. C., et al., *J. Am. Chem. Soc.* (2005) **127**, 14904
36. Yildirim, T., and Hartman, M. R., *Phys. Rev. Lett.* (2005) **95**, 215504
37. Debenedetti, P. G., and Stanley, H. E., *Phys. Today* (June 2003) **56**, 40
38. Stanley, H. E., *Mysteries of Water*, Bellissent-Funel, M.-C., (ed.), *NATO Science Series A Vol. 305*, IOS Press, Amsterdam, The Netherlands, (1999)
39. Teixeira, J., et al., *Phys. Rev. A* (1985) **31**, 1913
40. Singwi, K. S., and Sjölander, A., *Phys. Rev.* (1960) **119**, 863
41. Bellissent-Funel, M.-C., et al., *Phys. Rev. E* (1995) **51**, 4558
42. Zanotti, J.-M., et al., *Phys. Rev. E* (1999) **59**, 3084
43. Mitra, S., et al., *Solid State Commun.* (1998) **105**, 719
44. Swenson, J., et al., *J. Chem. Phys.* (2000) **113**, 2873
45. Swenson, J., et al., *J. Chem. Phys.* (2001) **115**, 11299
46. Mamontov, E., et al., *Phys. Rev. E* (2005) **71**, 061502
47. Paoli, H., et al., *Microporous Mesoporous Mater.* (2002) **55**, 147
48. Nair, S., et al., *Phys. Rev. B* (2005) **71**, 104301
49. Harpham, M. R., et al., *J. Chem. Phys.* (2004) **121**, 7855
50. Mamontov, E., *J. Chem. Phys.* (2005) **123**, 024706
51. Mamontov, E., *J. Chem. Phys.* (2004) **121**, 9087
52. Mamontov, E., *J. Chem. Phys.* (2005) **123**, 171101
53. Faraone, A., et al., *J. Chem. Phys.* (2003) **119**, 3963
54. Faraone, A., et al., *Euro. Phys. J. E* (2003) **12**, S59
55. Liu, L., et al., *J. Phys.: Cond. Matter* (2004) **16**, S5403
56. Faraone, A., et al., *J. Chem. Phys.* (2004) **121**, 10843
57. Liu, L., et al., *Phys. Rev. Lett.* (2005) **95**, 117802
58. Angell, C. A., *J. Non-Cryst. Solids* (1991) **131-133**, 13
59. Ito, K., et al., *Nature* (1999) **398**, 492
60. Kanno, H., et al., *Science* (1975) **189**, 880
61. Poole, P. H., et al., *Nature* (1992) **360**, 324
62. Prielmeier, F. X., et al., *Phys. Rev. Lett.* (1987) **59**, 1128
63. Bergman, R., and Swenson, J., *Nature* (2000) **403**, 283
64. Chen, S. H., et al., *Phys. Rev. E* (1999) **59**, 6708
65. Liu, L., et al., *Phys. Rev. E* (2002) **65**, 041506
66. Taylor, H. F. W., *Cement Chemistry*, Thomas Telford, London, UK, (1997)
67. FitzGerald, S. A., et al., *Chem. Mater.* (1998) **10**, 397
68. Berliner, R., et al., *Cem. Concr. Res.* (1998) **28**, 231
69. Faraone, A., et al., *J. Chem. Phys.* (2004) **121**, 3212
70. Fratini, E., et al., *J. Phys. Chem. B* (2002) **106**, 158
71. Fratini, E., et al., *Phys. Rev. E* (2002) **65**, 010201
72. FitzGerald, S. A., et al., *Cem. Concr. Res.* (2002) **32**, 409
73. Thomas, J. J., et al., *J. Am. Ceram. Soc.* (2001) **84**, 1811
74. Allen, A. J., et al., *J. Mater. Res.* (2004) **19**, 3242
75. Peterson, V. K., et al., *J. Phys. Chem. B* (2005) **109**, 14449
76. Peterson, V. K., et al., *Physica B* (2006), in press
77. Robinson, R. A., and Kennedy, S. J., *Physica B* (2002) **311**, 44
78. Gou, C., et al., *Physica B* (2002) **311**, 40
79. Shen, F., and Yuan, L., *Physica B* (2002) **311**, 152
80. Gläser, W., *Appl. Phys. A* (2002) **74**, s23
81. <http://j-parc.jp/MatLife/en/index.html>
82. Bennington, S. M., et al., *J. Neutron Res.* (2003) **11**, 93
83. Mason, T. E., et al., *Appl. Phys. A* (2002) **74**, s11